Chapter 4 Results and Discussion

4.1 The bifurcation diagram

In previous study (ref. [13]), we use the rate equations and Huygens' diffraction integral to simulation a plane-concave laser cavity. Laser will spontaneous instability under the adequate pumping spot around the $g_1g_2 = 1/4$ cavity configuration. There are something should be noted in our simulation, first we tune the cavity configuration by changing the radius of the output coupler, second the thermal effect is not considered here, and third, the rate equation only contain a gain saturation of the nonlinear effect.

From the simulation results (ref. [13]), we found that when the pump power is above some critical value so-called the V-shaped second threshold which will be discuss in the following section, the laser output became instability. Above the V-shaped bifurcation, we also found that there are several different dynamics in this laser system for different pumping power and cavity length, i.e. quasi-periodic, modulated quasi-periodic, precession oscillation, modulated pulsing and chaos, as shown in Fig. 4.1 (ref. [13]), where ρ is reflectivity of the electric field and Ψ is the ratio of pumping spot and beam waist of cavity mode which is 108 μm. The character of each dynamic behavior will be discussed in the following section.

The x-axis of Fig. 4.1 is the radius of the curvature of the output coupler. We fixed the cavity length L = 6cm, and tuning the curvature of the output coupler is equivalent to tuning g_1g_2. The y-axis on the left side is the pumping power, P_p. On the other side, that is the ratio of pumping power (P_p) and threshold power (P_1).

Because we simulate it without the thermal effect, the bifurcation diagram is symmetric to the 8 cm radius of the output coupler which is $g_1g_2 = 1/4$. So we only show one side of the diagram to present. In facts, the thermal effect will slightly

shift all the dynamics regions toward short cavity length which means the regions will shift to left-hand side in the Fig 4.1.

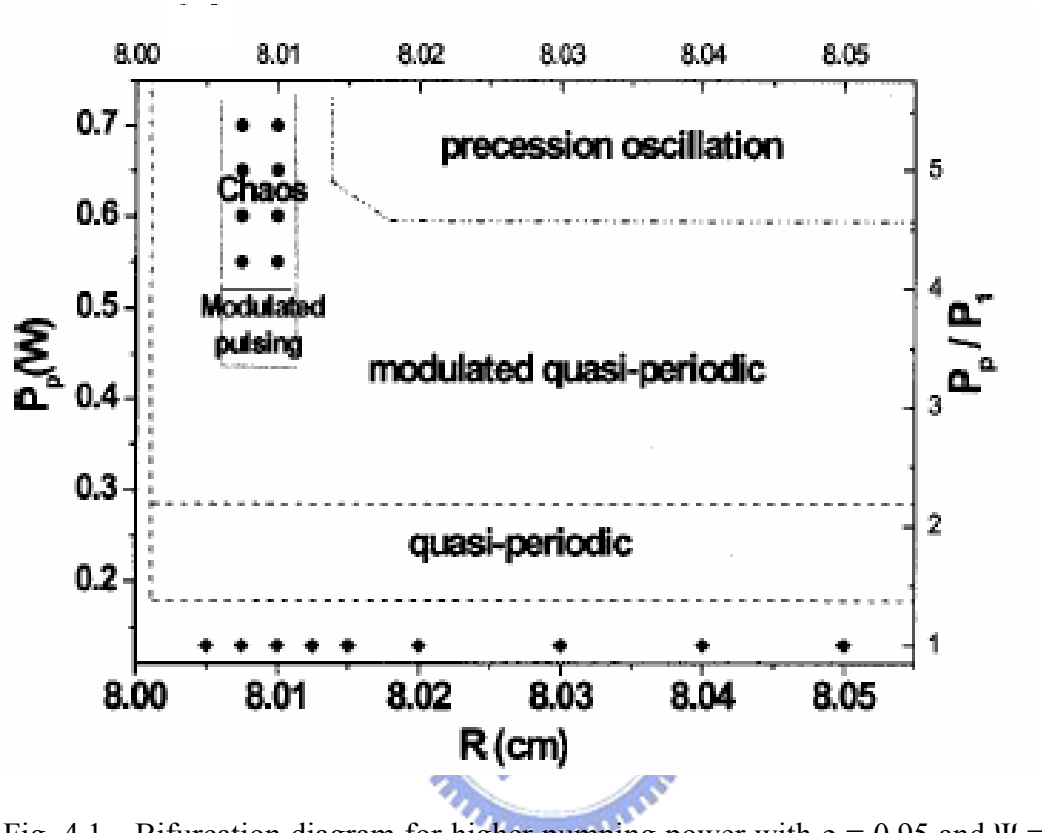

Fig. 4.1 Bifurcation diagram for higher pumping power with ρ = 0.95 and Ψ = 2.78 near $g_1g_2 = 1/4$

4.2 The second threshold to instability

Now, we introduce the thermal effect into our simulation model to further study the laser system as mentioned in the section 2.2 and 2.3. In previous section, we have known that if pump power exceeds a critical value laser output would become unstable. The critical value is the so-called second threshold to instability. In this section, we will discuss the bifurcation of the second threshold. We found that its

behavior not only depends on cavity configuration but also on the pumping spot size and cavity loss. We will discuss the simulation and experiment results as follow section.

4.2.1 The relation between the second threshold and the spot size

(a) Simulation

In the previous section, we knew that if pump power exceed some critical values, the laser output would become unstable and discuss the unstable behavior of each dynamics. Now we will study the threshold from stable to unstable output in simulation and experiment, respectively.

We found that the second threshold depends on several operation parameters such as the pumping spot size and the cavity length. Including the thermal effect in this simulation, we found the lowest second threshold for each spot size is located at different cavity length. Fig. 4.2 shows the second threshold as a function of pump spot size. By tuning the spot size from 350 μm to 150 μm, the second threshold first decreases to a critical value which shows minimum, then progressively increasing in second threshold. We found that the lowest second threshold happens at pumping spot size 200 μ m.

(b) Experiment

The corresponding experiment result is shown in Fig. 4.3. Similar to the simulation result, the second threshold decreases with decreasing the spot size until the spot size reaching the critical value. However, the observed second threshold just increases slightly and then almost keeps. Contrast, this may be due to incomplete compensation by the cylindrical lens

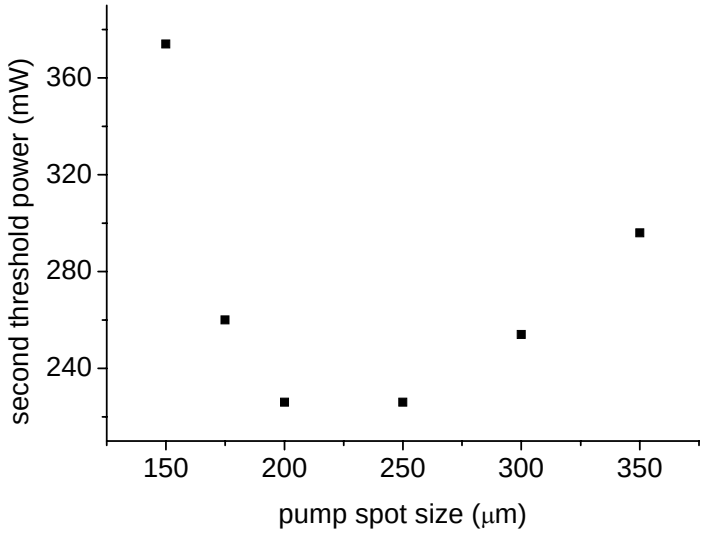

Fig. 4.2 The relation between pump spot size and second threshold in simulation

In. section 3.2.3, we had shown the spot size diagram for different distance between cylindrical lens and laser diode and left a question why we choose a asymmetric spot size. At the beginning, we hope to rearrange the light distribution to be symmetric. Unfortunately, it is impossible to make pump intensity distribution be perfect symmetric. However, for the spot size shown in Fig.3.3(a) the aspect ratio is too small to induce two group transverse mode families with different thermal effect in two axes, and then the laser output would be more complicated. So we try to find the spot size with a suitable aspect ratio to just induce one transverse group in only one direction. And the ratio of the spot size shown in Fig. 3.3(c) is about 2:1, and it should be a suitable spot size.

The reason of this contradiction is related to the asymmetry of the pump light distribution. The distribution of the pumping beam used in the experiment is shown in Fig. 4.4. The instability is induced by the interaction of the transverse modes that shows low frequency transverse mode beating. The number of the transverse modes excited depend on the pump spot size and pump power. The most transverse modes

are excited with the higher pump power and the larger spot size. The relation between the observed second threshold and spot size is shown in Fig. 4.3, where region of spot size is denoted by the ellipse in Fig. 4.4. From the Fig. 4.2, we know that when the spot size approaches 200μm, the second threshold would be the smallest. So we suppose that when we decrease the spot size of the x-axis the second threshold would decrease first and increase significantly, just like the result in simulation on Fig. 4.2. However, when the spot size of x-axis keeps decreasing from 200μm, the spot size of the other axis just passes through 400μm. As the spot size of the x-axis tune small, we thought that the second threshold would increases, but the spot size of the other axis is closer the value which the second threshold is the smallest, so the second threshold decreases again. This effect is due to asymmetry of the pump light, if we use symmetric pump light, we can avoid this contradiction.

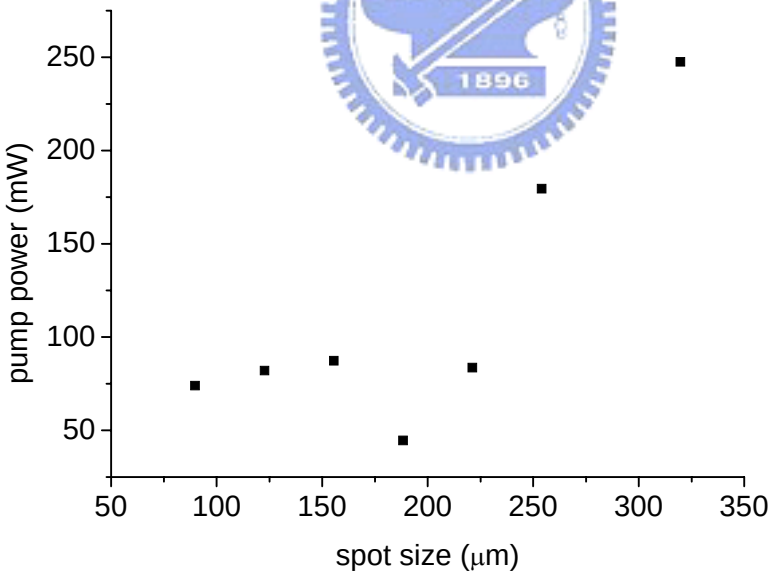

Fig. [4.3] The relation between pump spot size and second threshold in experiment

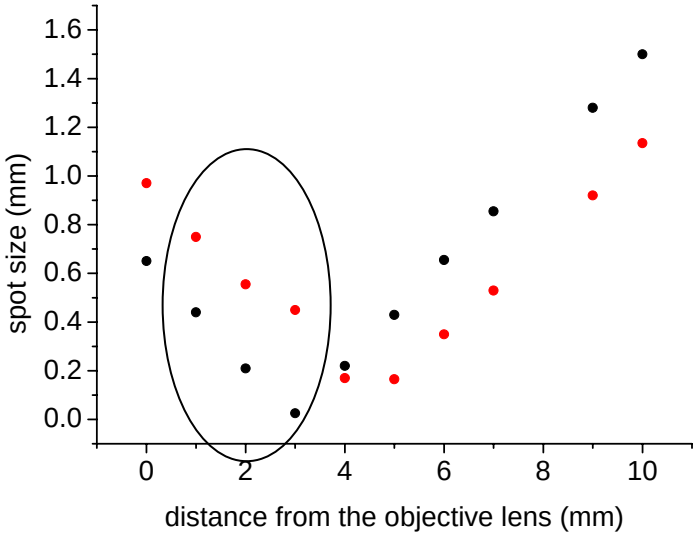

Fig. [4.4] The distribution of pump light in two axis.

4.2.2 The dependence of second threshold on the cavity configuration

(a) Simulation

In the previous section, we have known that when the pump power exceeds a critical value the laser output would become instability, and it will depend on the pump size. From previous study (ref. [13]), however, we also knew that the bifurcation of second threshold is not a smooth curve depend on the cavity configuration. In this section, we will study this character with the thermal lens effect.

We use the simulation model with slightly tuning the cavity length and pump power to find the instability in this system. As in Fig. 4.5, we found that the second threshold depends on the cavity length. At the degenerate, the second threshold is the smallest around L=6cm where is 1/3 degenerate. And the second threshold is higher as the cavity length is tuned away from the degenerate. So the second threshold diagram reveals a **V-shaped second threshold**. It should be noted that because of the thermal effect the position of the smallest second threshold is not

exactly at the degenerate, but slightly shifted toward the short cavity. The shift distance is about 20μm. It also worth to note is that the depth of the second threshold is not as deep as that without thermal effect (ref. [13]). We simulate this system with several spot sizes, and found that the depth of the second threshold depends on spot size, too. The smaller spot size, the deeper the depth is. For example, the depth is about 4mW for the spot size of 300μm; it becomes about 30mW for 150μm(Fig. 4.6).

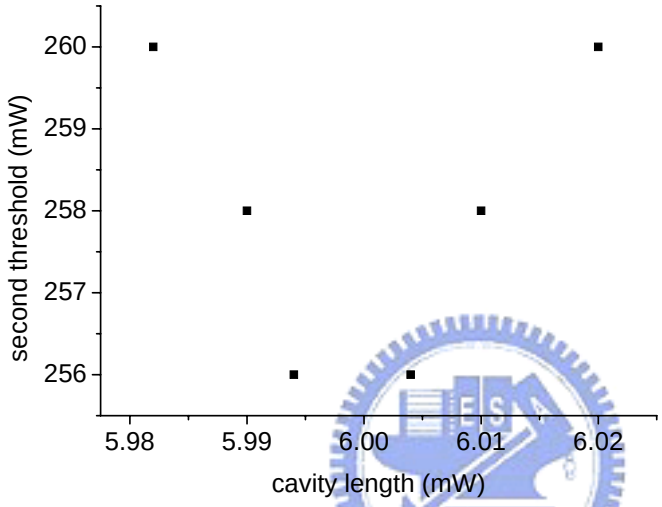

Fig. [4.5] The V-shaped second threshold in simulation for spot size = 300μm

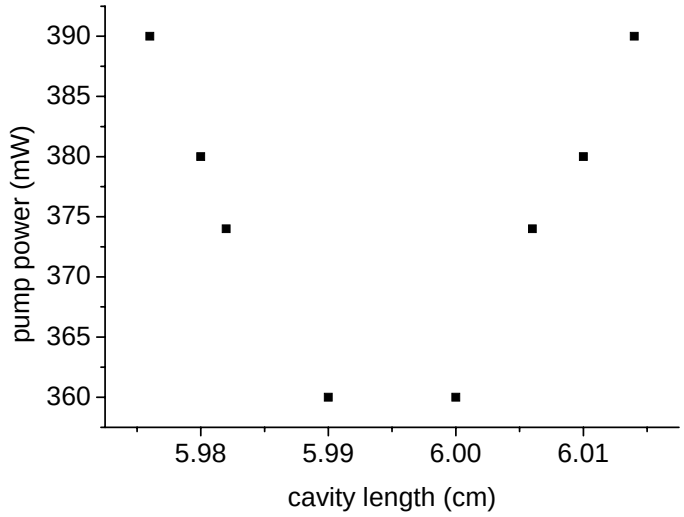

Fig. [4.6] The V-shaped second threshold in simulation for spot size = 150μm

(b) Experiment

We also show this behavior in Fig. 4.7 and Fig. 4.8. Fig. 4.7 shows the depth of V-shaped threshold is about 3 mW in experiment for spot size = 320 μm. Fig. 4.8 shows the same thing for 150 μm and its depth is about 30 mW. In the experiment, we observe the instability depend not only on the cavity configurations but also the thermal lens effect. This result agrees with simulation.

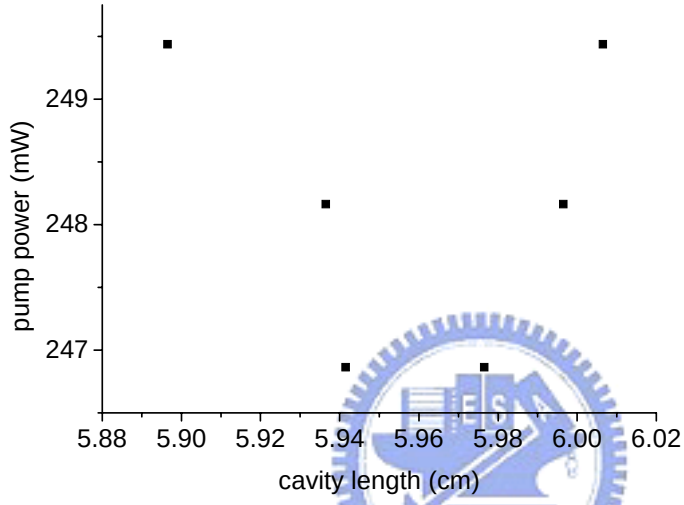

Fig. [4.7] The observed V-shaped second threshold for spot size of 300μm

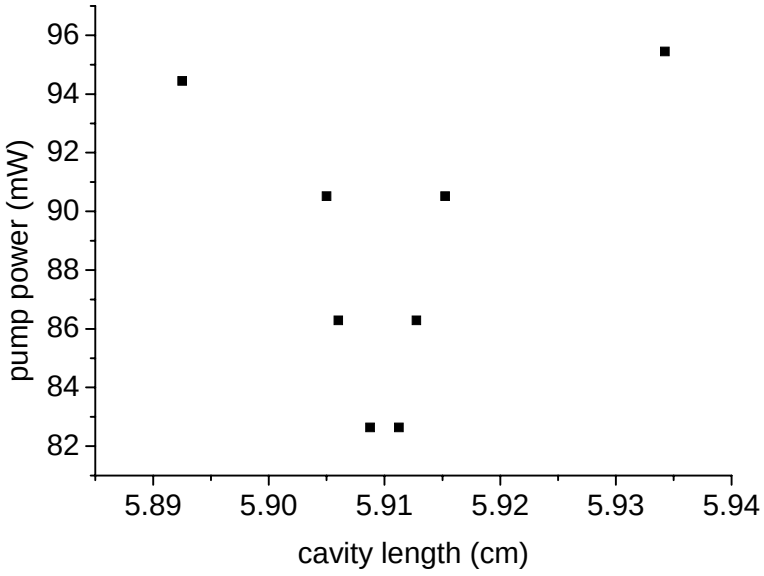

Fig. [4.8] The observed V-shaped second threshold for spot size of 150μm

4.2.3 The cavity loss

In the previous section, We have discussed the cavity configuration dependence of laser dynamics under the good cavity condition with reflection coefficient ρ = 0.95, we found the second threshold is not a smooth curve but a V-shaped. However, the laser is a high-loss cavity and uniformly pumping in Melnikov's research that has a continuously smooth quasi-periodic second threshold (ref. [3]). So we will study the influence of the output coupler reflectivity in this section.

To examine the influence of cavity loss in laser dynamics, we have studied the dynamics for ρ = 0.7746 for ω_p = 300μm, that corresponding reflectivity = 0.6. Shown in Fig. 4.9, we can see that the depth of the V-shaped threshold decrease which compare to the Fig. 4.5. The depth of the V-shaped is about 1.5mW, and smoothes the curve. This smooth curve is similar to the discussion in Ref. [3] for 50% mirror reflection. We know that the depth of the V-shaped second threshold depends on the output coupler reflectivity. Thus the V-shaped quasi-periodic threshold will not be found in the research reported in Ref. [3], where a high-loss cavity was considered, nor in Ref. [5-7], with uniform pumping.

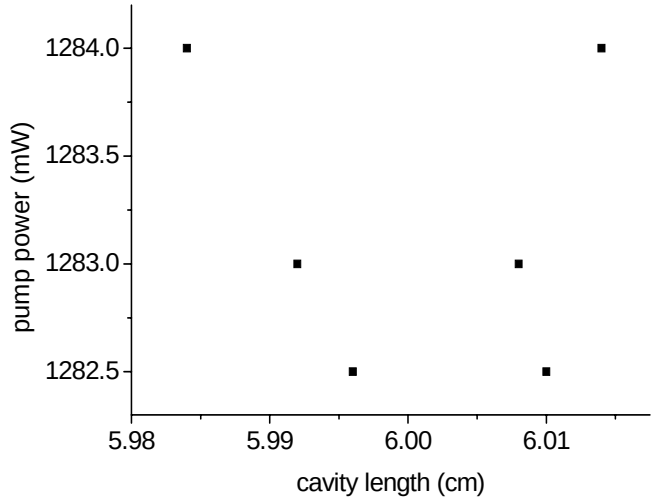

Fig. [4.9] The V-shaped second threshold in simulation for spot size of 300μm with R = 60%.

From the simulation result, we knew that the second threshold for R = 60% is about 1300 mW. In addition, the variation of the second threshold is extremely small 0.1% as compare with that of the low loss cavity which has almost 10% variation.

We have discussed the detail behavior of the V-shaped second threshold and summarize as follows. First, we knew the second threshold depends on spot size. The smallest second threshold happen at spot size about 200 μm. And we also found that the second threshold depends on the cavity configuration. At the degenerate, the second threshold is smallest around the L=6cm where is the 1/3 degenerate, and it become higher when cavity is tuned away from the degenerate. So the bifurcation diagram demonstrates **V-shaped second threshold**. Finally we studied the dependence of the depth of the V-shaped second threshold on the high-loss cavity loss and showed that it agrees with the result of Melnikov's (ref. [3])

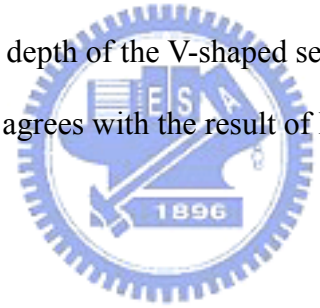

4.3 The dynamics of the laser system

In previous section, we had discussed the second threshold to instability and there are several kinds of dynamics in the laser system. In this section we describe each dynamics in this laser system with 300 μm spot size. In order to avoid confusing, we discuss them in simulation and experiment separately. The parameter we used below are L is the cavity length, ρ is the reflectivity of output coupler, and Ψ is the ratio of pumping spot size and cavity mode beam waist.

(a) Simulation

When the pump power just exceeds the second threshold, the laser output would become quasi-periodic, as shown in Fig. [4.10] and the corresponding magnification

portion in the inset.

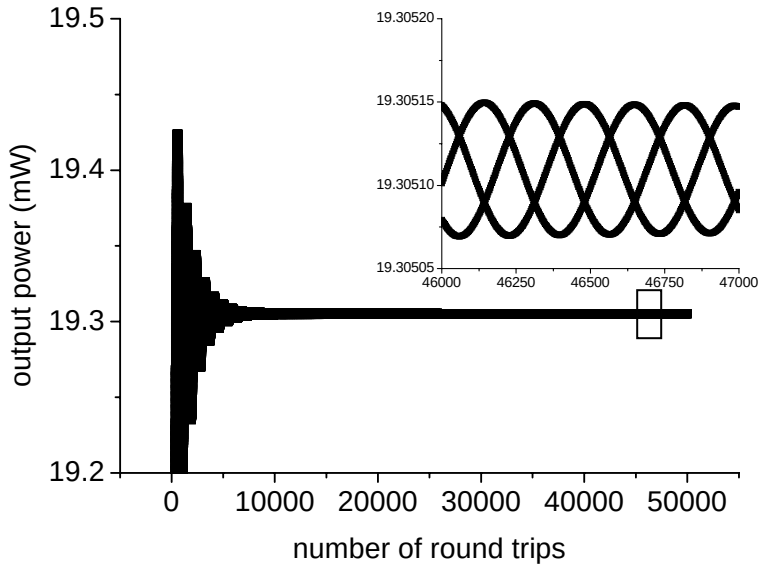

Fig. [4.10] Evolution of the output power of the quasi-periodic oscillation with and pump power = 264 mW and L = 6.02 cm, $\rho = 0.95$, $\Psi = 2.78$. The inset is the magnification of final 3000 round trips.

From the figure, we found that there is an obviously relaxation oscillation at the beginning of 5000 round trips, and then the output damps out but will not reach a stable output as a quasi-periodic oscillation which shows in the inset. The modulation depth is almost on parts in millions of the average power output. It should be noted that, the modulation depth of CW laser is 10^{-10} not 0 which corresponds to the added spontaneous noise. In the figure, we use the round trip time as the x – axis, the time interval of each point is a round trip time that corresponds to the reciprocal frequency of 24.GHz. And we found that the output signal is three sinusoidal oscillations with same frequency range. So, there are a 1/3 longitudinal mode beating signal in the output signal about 800 MHz.

Keep increasing the pump power, to 450 mW at L = 5.988 cm, we found a different dynamics called as modulated quasi-periodic shown as (Fig. [4.11]). At the first sight, we may think that dynamics is an irregular oscillation. However, from the power spectrum we found that there is a low frequency peak which modulates the laser output. The other feature of modulated quasi-periodic is the modulation depth of it is larger than quasi-periodic which is about 2%.

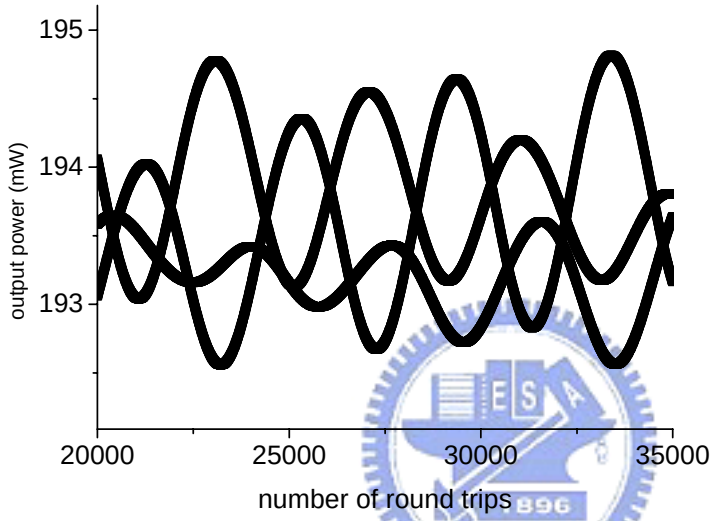

Fig. [4.11] power evolution of modulated quasi-periodic with pump power = 0.45W, Ψ = 2.78, L = 5.988 cm

Slightly tune the cavity far away from degenerate to L = 5.984 cm, we still find the quasi-periodic dynamics and it gradually change to the modulated quasi-periodic at 1W pumping. Further increasing the pump power slightly, the modulation suddenly becomes large with 45% depth, shown in Fig. 4.12. It should be noted that the high frequency oscillation disappear the leads to 4.7MHz oscillation, which is not corresponding to the relaxation frequency but a so-called precession frequency. We will discuss the precession frequency in the following section.

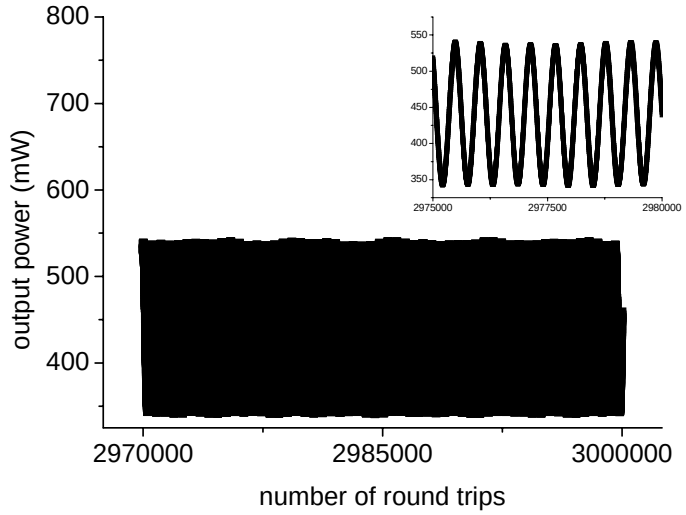

Fig. [4.12] power evolution of precession oscillation with pump power = 1W, Ψ = 2.78, L = 5.984 cm

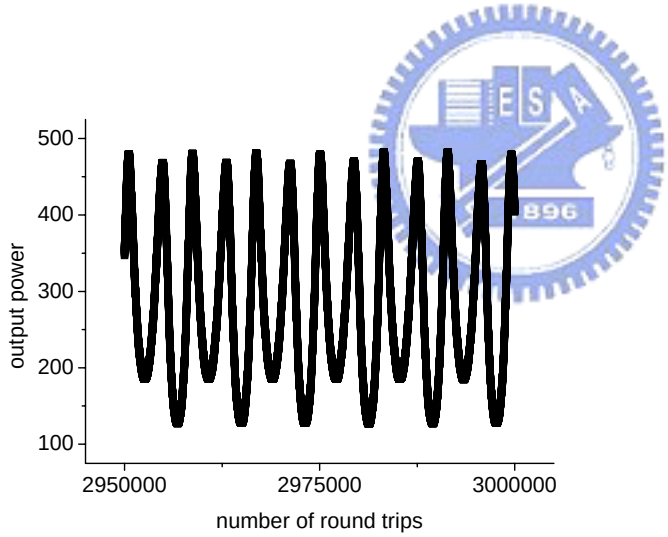

Fig. 4.13 power evolution of pulsation in simulation pump power = 600 mW, Ψ = 2.78, L = 6.004 cm

By setting the cavity around L = 6.004 cm, dynamics called modulated pulsing is shown in Fig. 4.13. We found that dynamics at lower pump power at 600 mW. From the bifurcation diagram in Fig. 4.1 we know that this dynamical behavior only exits in a very narrow range. At the same cavity length, further increasing the pump

power to 1W we will find the dynamics with chaotic output shown in Fig. 4.14.

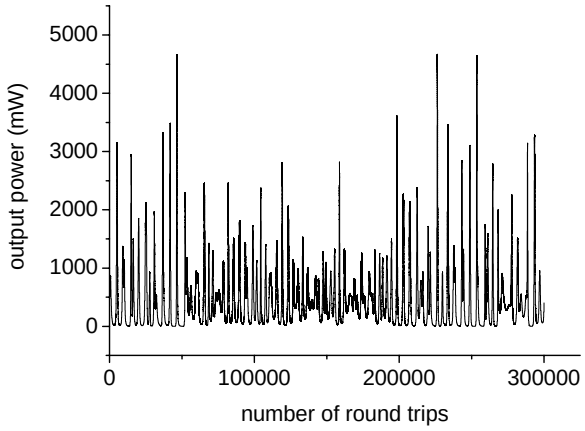

Fig. 4.14 power evolution of chaos in simulation pump power = 1W, Ψ = 2.78, L = 6.004 cm

(b) Experiment

Here we will show our experiment observations of these several dynamics mentioned in the simulation.

First, for pump power just above the second threshold, we found the similar dynamics of modulated quasi-periodic. In the simulation, we use FFT to analyze power evolution, and there is about 20MHz and 800MHz peak corresponding to the 1/3 of the longitudinal frequency. We found a low frequency signal about 20 MHz in RF spectrum as Fig. [15]. However, we can not record it on the oscilloscope because of too small modulation depth.

Further increasing the pump power, we obtained the precession oscillation with frequency of about 42 MHz, shown in Fig. 4.16 (a) and (b). The signal is close to a sinusoid, but because of the sampling of the oscilloscope, so the curve in Fig. 4.16 (a) is not a perfect sinusoid wave. The modulation depthis about 32%.

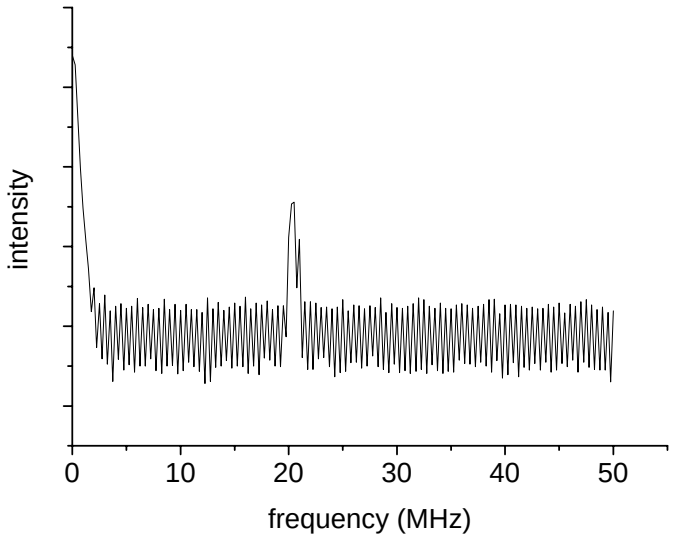

Fig. 4.15 The frequency distribution of quasi-periodic

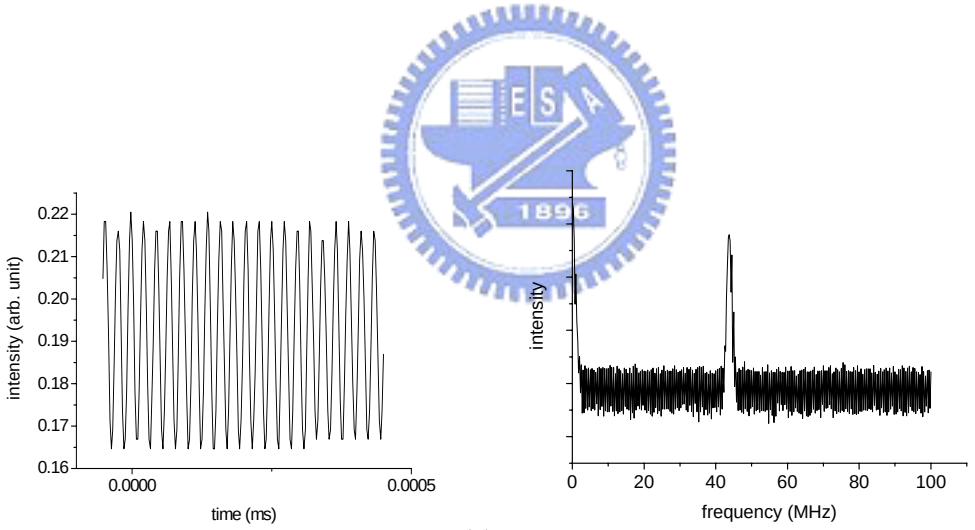

(a) (b)

Fig. 4.16 power evolution (a) and spectrum (b) of precession oscillation in experiment

When we slowly decrease the cavity length and keep the same pump power, the precession frequency decreases as the cavity is tuned closer to the degenerate. The pulsation output near the degenerate configuration is shown as Fig. 17 (a) and (b). It is obvious that the power evolution of pulsation is similar to that of precession, but the modulation depth has reached about 98.3% with shaped peaks in time trace. The

spectrum of pulsation shows low frequencies about 1MHz and their harmonics that differ from that of precession oscillation.

Further slightly decreasing the cavity length, even closer to the degenerate. We found chaotic output and its broad band low frequency as Fig. 4.18 (a) and (b).

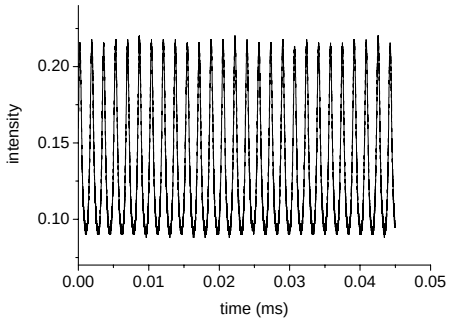

(a)

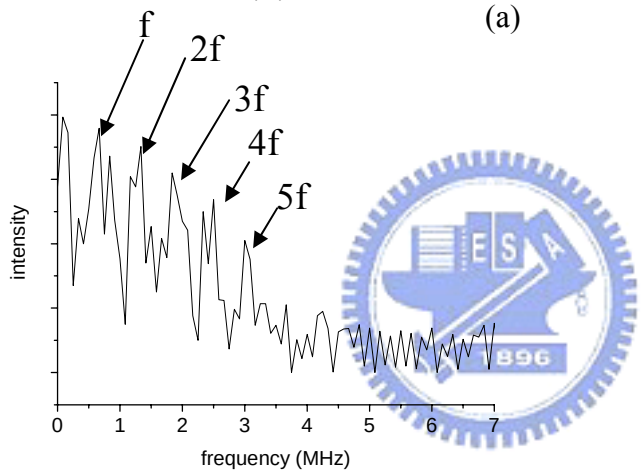

(b)

Fig. 4.17 power evolution (a) and spectrum (b) of pulsation in experiment

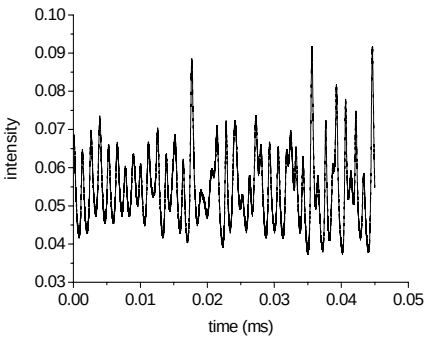

(a)

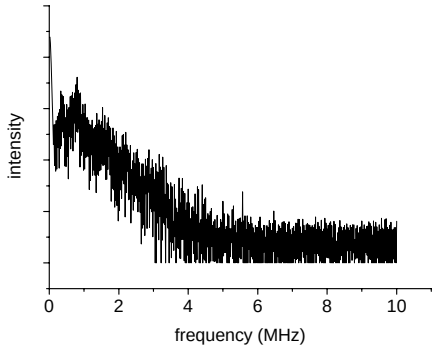

(b)

Fig. 4.18 power evolution (a) and spectrum (b) of chaos in experiment

4.4 Precession oscillation frequency

From section 4.1, we knew that if we maintain proper pump power and scan over the cavity on each side of the degenerate we will obtain instability of precession oscillation. In this section, we try to find out the course of the precession oscillation experimentally. We found that when we decrease the cavity length from long cavity side toward the degeneracy, the precession frequency decreases linearly. And the laser output will become chaotic when the cavity is close to degenerate. Further decreasing the cavity length, the precession oscillation appears again. After passing through the degeneracy, the precession frequency will increase with further decreasing the cavity length.

The character of the precession frequency depends on cavity length is similar to the transverse mode beating. We therefore plot a figure of precession frequency versus the cavity length as Fig. 4.19. It shows the frequency linear depend on the cavity length. Noted that, we determined the degenerate configuration by finding the position where the threshold is lowest. We fit the measured precession frequency curve linearly and found the slope of the precession frequency is about 316.95 MHz/cm, that is approximately equal to the transverse beat frequency between $HG_{n,30}$ and $HG_{n+1,00}$ of the cold cavity of about 320 MHz/cm. So, we presume that the precession frequency is due to transverse mode beating.

However, we also found a contradiction between our precession and cold cavity beat frequency. For a cold cavity, the beat frequency would be zero when cavity length is 6cm, that is, $g_1g_2 = 1/4$. If we extend the precession frequency to the frequency, the cavity length is not 6 cm. We believe this shift is induced by the thermal effect.

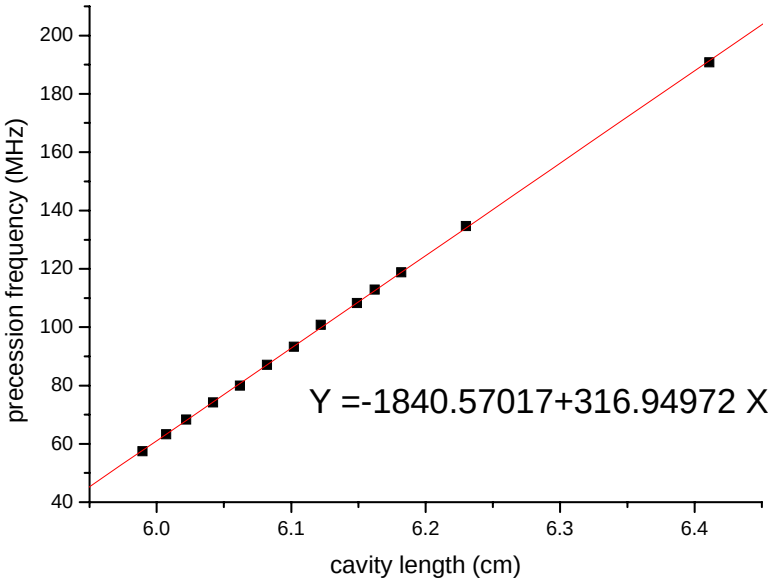

fig. 4.19 the precession frequency versus L for fixed pump power.

4.5 Chaos analysis

In time domain, the power evolution in Fig. 4.18 seems to be chaotic. We therefore use a software called as chaotic data analyzer program which can analyze the nonlinear dynamical data to make sure whether it is chaos or not. We import our data of the Fig. 4.18 to this program to calculate its correlation dimension. The plot of the correlation dimension versus the embedding dimension for both simulation ans measured data. We can know that how many dimension needed to describe a system. So the curve should be approach to some value.

Because of sampling by oscilloscope, there is always noise in our experiment data. This noise will affect our analyzing result. We must eliminate the noise. Import the data in “Origin” program. The measured curve with fluctuation as Fig. 4.20(a) can be smoothed out as Fig. 4.20(b). then we export the smoothed data to the

chaotic data analyzer program.

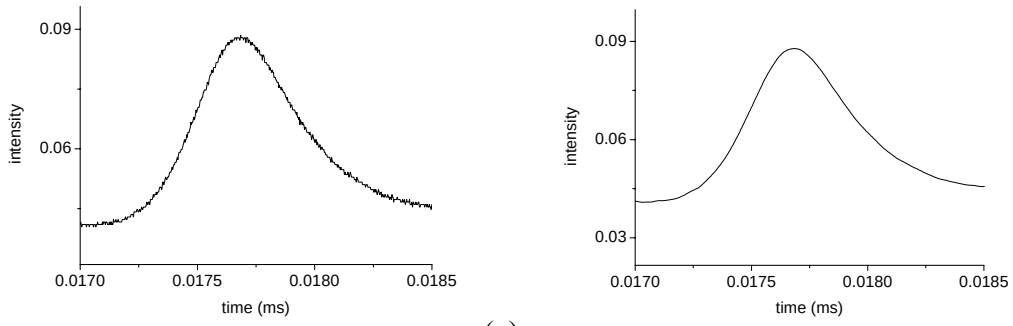

(a) (b)

Fig. 4.20 The data of chaos signal measure by oscilloscope (a) before smoothed and (b) after smoothed

We show the correlation dimension of both simulation and experiment data in Fig. 4.21 (a) and (b). We found the correlation dimensions converge between 1 and 2 for the simulated data, whereas, that of measured data converges between 2 and 3. The results present that both of them are fractal dimension. This is a important character of chaotic signal.

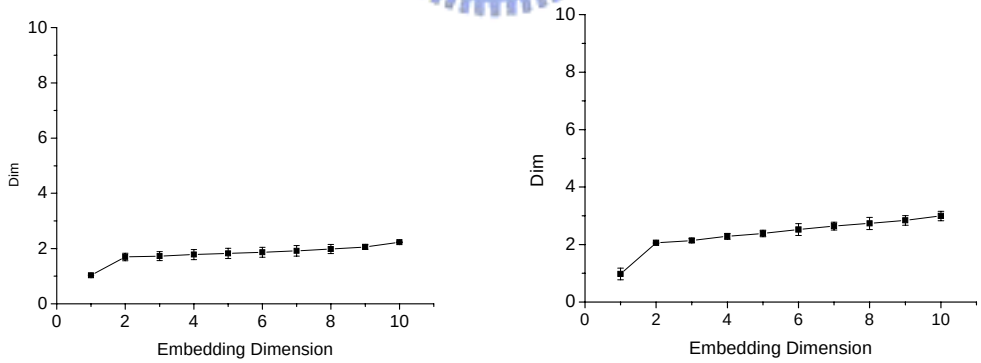

(a) (b)

Fig. [4.21] The correlation dimension of the system in simulation (a) and experiment (b)

4.6 Power bump and chaotic region

In this section we discuss the relation between the output power and cavity length, also observe the chaotic region in the laser system.

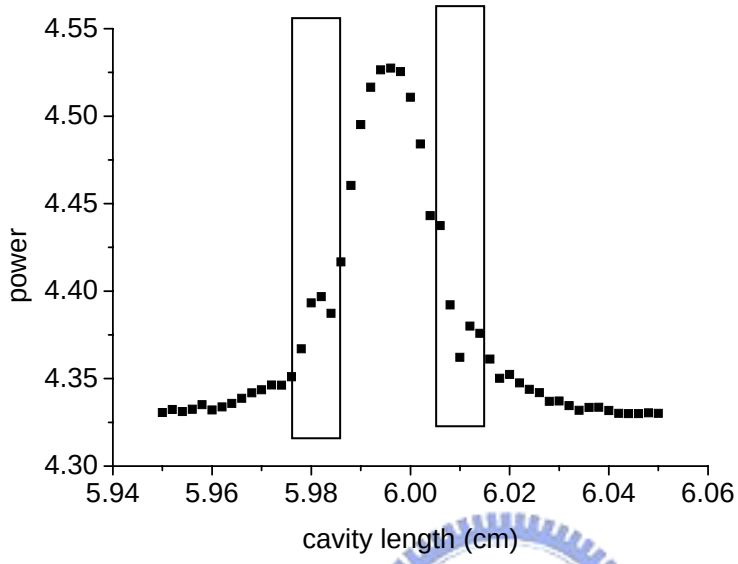

Fig. 4.22 Power bump and chaotic region in simulation

In simulation, we fixed the pump power at 1W and spot size of 300 μm. Scan the cavity from 5.94cm to 6.06 cm, and record the output power, we search for the chaotic region as Fig. 4.22. The maximum output power should be at degenerate configuration, but the simulation result slightly shifts due to the thermal effect. The chaotic regions are both two sides of the degenerate, this agrees with the result in section 4.1. And the chaotic regions are 5.978cm to 5.986 cm and 6.005cm to 6.015cm, respectively.

In experiment, we fixed the pump power at about 231 mW that we observe the precession oscillation, and scan the cavity from 5.8 cm to 6.2 cm. We can observe two chaotic regions between 6.015cm and 6.02cm and 6.072cm and 6.082cm and also measure the power bump, shown as Fig. 4.23. The shift again is due to thermal effect. Because of different thermal loading introduced in the simulation and experiment by

not well controlling described in chapter 3, the cavity shifts are different.

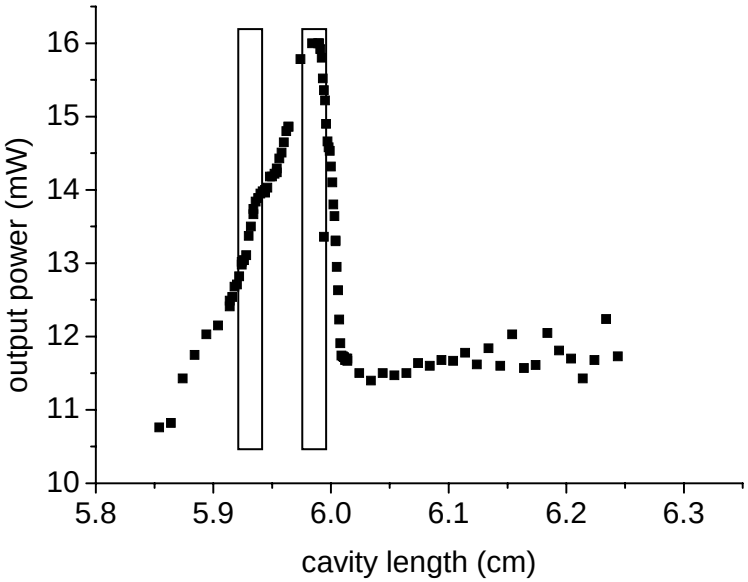

Fig. 4.23 Power bump and chaotic region in experiment